Research Square

Preprints are preliminary reports that have not undergone peer review.
They should not be considered conclusive, used to inform clinical practice,
or referenced by the media as validated information.

How consistent are landscape–cooling relationships across observations? Multidimensional ECOSTRESS evidence from the Beijing–Tianjin–Hebei region

Xiaofan Jiang
107081@hsu.edu.cn

Huangshan University
Jian Pan
Huangshan University
Haitao Wang
Tianjin Chengjian University
JP Liang
Huangshan University
Wen Zhou
Yangzhou University
Yan Yang
Tianjin Chengjian University

Article

Keywords: Urban green spaces, multidimensional cooling, landscape–cooling relationships, cross-observation consistency, nonlinear and conditional relationships

Posted Date: November 9th, 2026

DOI: https://doi.org/10.21203/rs.3.rs-11359616/v1

License: This work is licensed under a Creative Commons Attribution 4.0 International License.
Read Full License

Additional Declarations: No competing interests reported.

Abstract

Landscape–cooling relationships identified from individual thermal observations are often interpreted as planning evidence, yet their consistency across observations and cooling dimensions remains unclear. Rather than identifying influential factors within individual observations, this study evaluates how consistently landscape–cooling associations recur across heterogeneous observations and cooling dimensions. Using 126 urban green spaces (UGS) in the Beijing–Tianjin–Hebei region, we integrated four ECOSTRESS observations with landscape and urban variables. A Gaussian surface model quantified cooling intensity, distance, and efficiency, while random forest, SHAP, and partial dependence analyses evaluated their recurrence, nonlinearity, and conditionality. Cooling magnitude and heterogeneity varied substantially across observations, with the lowest values at 00:31 and the highest at 10:50 across all three cooling dimensions. Green-space area showed the most recurring and predominantly positive association, whereas vegetation condition, spatial cohesion, and morphological and contextual factors were more observation- or dimension dependent. Even recurring associations were nonlinear and conditional; area showed diminishing marginal gains around 20 ha in several models, while vegetation responses varied across structural and contextual combinations. These findings show that cross-observation consistency is a matter of degree and support distinguishing recurring from context-dependent evidence for differentiated UGS planning.

1 Introduction

Urban warming has become an increasingly important challenge for climate-resilient urban development as climate change and continued urbanization intensify thermal stress in cities [1]. Persistent urban heat can increase human exposure to thermal stress and associated health risks, particularly for populations with limited physiological or adaptive capacity [2, 3]. Urban green spaces (UGS) provide an important nature-based response by modifying surface energy exchange through vegetation shading and evapotranspiration [4]. Their capacity to mitigate local heat has therefore become an important consideration in urban climate adaptation and landscape planning [5]. However, the cooling performance observed for a green space is not necessarily a fixed property. It may vary with thermal background conditions and the timing of observation, raising an important question for planning: how robust is the cooling-related evidence derived from any single thermal observation?

Previous studies show substantial temporal and environmental variation in UGS cooling. Cooling intensity, distance, and efficiency vary with seasonal radiation, vegetation activity, and surrounding thermal conditions [6], while vegetation-related cooling also depends on background temperature and humidity [7]. Urban form–temperature relationships can differ between daytime and nighttime observations [8], and ECOSTRESS-based studies likewise report variation in park cooling among observation times [9]. Thus, individual thermal scenes should not be treated as fixed representations of cooling performance. Cooling performance also varies with green-space characteristics and surrounding urban context. Green-space size is widely reported as important, but its cooling relationship is often nonlinear and scale-dependent [10, 11]. Spatial configuration also matters, although the direction and

strength of individual landscape-metric relationships vary among studies [12], with area, vegetation condition, shape, and aggregation contributing differently [13]. Surrounding building density, floor-area ratio, and other urban-form characteristics can further affect cooling magnitude and propagation [14], while the effects associated with UGS characteristics may vary with urban context [15]. Together, these findings suggest that landscape–cooling relationships are unlikely to remain uniform across observational, structural, and contextual settings.

Machine-learning approaches increasingly characterize nonlinear and multivariable relationships between green-space or urban morphology and thermal outcomes [16, 17]. Interpretable methods further reveal the direction, nonlinearity, and conditionality of individual relationships: RF–SHAP analyses show that variable contributions can depend on other urban and meteorological factors [18]. Despite these methodological advances, most existing studies still identify influential landscape attributes within particular observation conditions, cities, seasons, or cooling metrics. Consequently, considerably less is known about whether the resulting landscape–cooling relationships recur when cooling is evaluated across heterogeneous observations and multiple cooling dimensions. Moreover, even comparatively recurring associations may not be uniformly expressed: their magnitude may be nonlinear, and their contribution may depend on other aspects of landscape structure or surrounding urban context. Thus, the key issue is not simply which landscape attributes are associated with UGS cooling, but how consistently these associations are expressed across observations and cooling dimensions, and under what conditions they change.

Against this background, taking the Beijing–Tianjin–Hebei (BTH) urban agglomeration as the study area, this study shifts the analytical focus from identifying influential factors under individual observations to evaluating the consistency and conditionality of multidimensional landscape–cooling relationships across multiple ECOSTRESS observations. Specifically, the study addresses three related questions: (1) How does multidimensional UGS cooling performance, in terms of cooling intensity, cooling distance, and cooling efficiency, vary across ECOSTRESS observations? (2) Which landscape–cooling associations remain relatively consistent across observations and cooling dimensions, and which vary with observation conditions or the dimension of cooling being evaluated? (3) How do nonlinear responses and conditional relationships shape the associations between key landscape attributes and UGS cooling performance, and what do these patterns imply for context-sensitive green-space planning?

2 Study area and dataset

2.1 Study area

This study focuses on the Beijing–Tianjin–Hebei (BTH) urban agglomeration (Fig. 1), a rapidly urbanizing region experiencing substantial summer heat stress. Between 2000 and 2020, the region experienced, on average, more than ten heat-wave days per year, with the duration of high-temperature events increasing by approximately 30% compared with the early 2000s [19]. The four representative cities included in this study—Beijing, Tianjin, Shijiazhuang, and Baoding—differ in their urban and geographical settings. Beijing

lies at the transition between mountains and plains, Tianjin is influenced by coastal conditions, Shijiazhuang represents a high-density inland city, and Baoding is a rapidly urbanizing plain city [20]. These contrasting settings provide a suitable regional context for comparing UGS cooling and landscape–cooling associations across heterogeneous observations.

A total of 126 UGS samples were selected across the four cities. Their boundaries were delineated through visual interpretation of GLC_FCS10 land-cover data [21] and Google Earth high-resolution imagery and were subsequently validated using local government planning datasets. To reduce potential interference from scale, water bodies, external cooling sources, and land-cover change, each UGS was required to meet four criteria: (1) area > 1 ha, avoiding unstable cooling estimates associated with very small green spaces [11, 22]; (2) internal water coverage < 5%, limiting cooling effects dominated by water bodies [23, 24]; (3) sufficient separation from major water bodies and mountainous terrain to reduce interference from external cooling sources [25]; and (4) stable land-cover conditions throughout the study period, verified using multi-temporal historical imagery [26].

2.2 Data collection

Land surface temperature (LST) data were obtained from the NASA ECOSTRESS ECO_L2_LSTE product at a spatial resolution of 70 m, which is generated using the temperature and emissivity separation algorithm [27]. Given the irregular overpass schedule and data availability of ECOSTRESS, observations were screened according to data quality and spatial coverage. Four observations providing adequate coverage of the study area and meeting the quality-control requirements were retained: 00:31 on September 20, 2022; 07:37 and 10:50 on August 22, 2024; and 16:37 on July 23, 2023. Because these observations were acquired on different dates and in different years, they were treated as independent observation windows under heterogeneous conditions rather than as a continuous temporal or diurnal sequence. The retained scenes showed no obvious cloud contamination or precipitation-related disturbance based on the applied quality-control screening [28], and no spatial interpolation or data imputation was performed. After quality control, all LST data were reprojected to WGS 84/UTM Zone 50N and extracted for subsequent UGS cooling analysis. Previous validation studies have reported an RMSE of approximately 1–3 K for ECOSTRESS LST products [29]. The ECOSTRESS data were obtained through NASA JPL AppEEARS, with all data sources summarized in Table 1.

Table 1
Data sources

Data type	Data feature	Data source
ECOSTRESS LST	Raster, 70 m, with QC flags	NASA JPL AppEEARS (https://appeears.earthdatacloud.nasa.gov/)
Landsat-8 OLI surface reflectance	Raster, 30 m, 2023	Google Earth Engine (Landsat Collection 2 Surface Reflectance)
GLC_FCS10 land-cover dataset	Raster, 10 m, 2023	Aerospace Information Research Institute, CAS (GLC_FCS10 dataset)
Building footprint and height data	Vector, building geometry and height, 2023	Gaode Map (AMap) (https://www.amap.com/)
Population density	Raster, population counts, 2023	WorldPop (China 2023 Population Counts)

Explanatory variables were organized into four categories: blue-green factors, internal geometry, morphological ventilation, and external urban context (Table 2). To characterize both UGS properties and the surrounding conditions potentially associated with cooling propagation, variables were derived for two spatial domains: the internal green space and the surrounding influence zone. This distinction reduces potential spatial mismatch associated with representing internal and external landscape conditions within a single fixed spatial unit [30, 31]. To maintain a consistent temporal reference across the explanatory dataset, 2023 was used as the common reference year. As this year falls within the 2022–2024 ECOSTRESS observation period, the approach reduces, although does not eliminate, temporal mismatch between cooling observations and explanatory variables. NDVI, albedo, and water proportion were derived from Landsat-8 OLI surface reflectance data; landscape metrics were calculated from the GLC_FCS10 land-cover dataset using FRAGSTATS; building height and floor-area ratio were derived from building footprint and height data; and population density was obtained from WorldPop.

Table 2
Explanatory variables for UGS cooling analysis

Categories	Variables	Formula	Description
Blue-green factors	Normalized difference vegetation index (NDVI_in)	$\mathrm{NDVI_in} = \frac{\mathrm{NIR}-\mathrm{RED}}{\mathrm{NIR}+\mathrm{RED}}$	Mean NDVI within UGS, spectral indicator of vegetation greenness. Range: −1–1.
	Water proportion (PW_in)	$\mathrm{PW_in} = \frac{A_{\mathrm{water}}}{A_{\mathrm{UGS}}}$	Proportion of water-body area within UGS. Range: 0–1.
	Albedo (Albedo_in)	$\mathrm{Albedo_in} = \frac{\sum(\mathrm{Reflected\ Radiation})}{\sum(\mathrm{Incoming\ Radiation})}$	Mean surface albedo within UGS, ratio of reflected to incoming shortwave radiation. Range: 0–1.
Internal geometry	Area (Area_in)	-	Total area of UGS patch. Unit: ha.
	Patch density (PD_in)	$\mathrm{PD_in} = \frac{n_{\mathrm{patch}}}{A_{\mathrm{UGS}}}$	Patch density within UGS, number of patches per unit area. Unit: n/ha.
	Landscape shape index (LSI_in)	$\mathrm{LSI_in} = \frac{\sum_{i=1}^{n} E_i}{2\times\sqrt{\pi\times\sum_{i=1}^{n} A_i}}$	Landscape shape index, standardized edge length adjusted for total area. Range: ≥1.
	Cohesion (Cohesion_in)	$\mathrm{Cohesion_in} = \left[1-\frac{\sum p_{ij}}{\sum p_{ij}\times\sqrt{a_{ij}}}\right]\times\frac{1}{\left(1-\frac{1}{\sqrt{Z}}\right)}\times 100$	Patch cohesion index, measuring physical aggregation of patches. Range: 0–100.
Morphological ventilation	Sky view factor (SVF_in)	$\mathrm{SVF_in} = \frac{1}{2}\sum_{j=1}^{m}\mathrm{SVF}_j$	Mean sky view factor within UGS, proportion of sky hemisphere visible from surface. Range: 0–1.
	Edge density (ED_out)	$\mathrm{ED_out} = \frac{\sum_{i=1}^{n} E_i}{A_{\mathrm{buffer\ zone}}}$	Edge density in buffer zone, total edge length per unit area. Unit: m/ha.
	Building height (BH_out)	$\mathrm{BH_out} = \frac{\sum_{i=1}^{n} H_i}{A_{\mathrm{buffer\ zone}}}$	Mean building height in buffer zone. Unit: m.

Categories	Variables	Formula	Description
External urban context	Floor area ratio (FAR_out)	$\mathrm{FAR_out} = \frac{1}{A_{\mathrm{buffer\backslash:zone}}} \times \sum_{i=1}^{n} (C_i \times F_i)$	Floor area ratio in buffer zone, total gross floor area relative to land area.
	Albedo (Albedo_out)	-	Mean surface albedo in buffer zone, representing solar radiation reflectivity. Range: 0–1.
	Normalized difference vegetation index (NDVI_out)	-	Mean NDVI in buffer zone, spectral indicator of vegetation greenness. Range: -1–1.
	Population density (POP_out)	$\mathrm{POP_out} = \frac{\mathrm{POP}}{A_{\mathrm{buffer\backslash:zone}}}$	Population density in buffer zone. Unit: persons/km².

3 Methods

3.1 Research framework

To examine multidimensional UGS cooling and the consistency and conditionality of its landscape associations across ECOSTRESS observations, this study developed a five-step analytical framework (Supplementary Fig. S1). First, multi-source remote-sensing and geospatial data were integrated to characterize thermal conditions, UGS attributes, and surrounding urban context. Second, GSCI, GSCD, and GSCE were quantified using a Gaussian surface model. Third, explanatory variables were organized into four categories: blue-green factors, internal geometry, morphological ventilation, and external urban context. Fourth, RF, SHAP, and partial dependence analyses were used to evaluate variable contributions, association directions, nonlinear responses, and conditional relationships. Finally, results were compared across observations and cooling dimensions to distinguish relatively recurring landscape–cooling associations from observation- and dimension-dependent patterns and to interpret their implications for context-sensitive UGS planning.

3.2 Cooling effect index calculation

This study employed a Gaussian surface model (GSM) to characterize the magnitude and spatial attenuation of UGS cooling. Originally developed to represent urban heat islands as two-dimensional Gaussian surfaces superimposed on a planar background [32], the GSM has subsequently been applied to characterize the intensity, spatial extent, and morphology of urban thermal anomalies [33, 34] and, more recently, UGS cooling effects [35]. Here, an anisotropic GSM was used to provide a continuous

representation of spatial temperature contrasts and derive GSCI, GSCD, and GSCE within a common modeling framework.

First, a spatial temperature-contrast field was constructed from the LST data. Let $\mathrm{T}(\mathrm{x},\mathrm{y})$ denote the pixel-wise LST at location (x,y), and $\mathrm{T}_{\mathrm{ref}}$ the mean LST of the surrounding reference area outside the UGS. The reference area was defined as a ring-shaped buffer outside the UGS boundary using a consistent rule for all samples, with the mean LST of valid pixels representing the local thermal background. Pixels affected by cloud contamination or precipitation-related disturbance were excluded during quality control. The temperature-contrast field was defined as:

$$\mathrm{C}\left(\mathrm{x},\mathrm{y}\right)=\backslash:\mathrm{T}_{\mathrm{ref}}-\mathrm{T}\left(\mathrm{x},\mathrm{y}\right)$$

1

Positive values therefore indicate cooler surface conditions relative to the surrounding reference background. To enable comparison among UGS of different sizes, an effective diameter was used to represent the characteristic spatial scale, calculated as the diameter of a circle with an area equivalent to that of the UGS.

Second, an elliptical Gaussian surface was fitted to the temperature-contrast field. Let $(\mathrm{x}_0,\mathrm{y}_0)$ denote the fitted center, a and b the scale parameters along the two principal axes, φ the rotation angle, and I_0 the fitted cooling amplitude. The anisotropic Gaussian surface was expressed as:

$$\widehat{\mathrm{C}}\left(\mathrm{x},\mathrm{y}\right)=\mathrm{I}_0\exp\left(-\frac{1}{2}\mathrm{Q}\left(\mathrm{x},\mathrm{y}\right)\right)$$

2

An elliptical normalized radius ρ was then introduced so that equal radius values corresponded to equal-valued elliptical isolines. The equivalent UGS boundary radius ρ_{b} was determined using an area-preserving condition:

$$\rho_{\mathrm{b}}^2=\frac{\mathrm{A}}{\pi\mathrm{ab}}$$

3

Third, a minimum detectable cooling threshold τ was introduced to distinguish meaningful modeled cooling from near-zero fluctuations after Gaussian smoothing. In this study, $\tau=0.1\backslash:\mathrm{k}$ was used as a conservative analytical threshold for consistently delineating the outer detectable cooling extent across all samples, rather than as a universal physical threshold. Setting the fitted Gaussian surface equal to this threshold yielded the corresponding normalized radius:

$$\rho_\tau^2 = 2\ln\left(\frac{\mathrm{I}_0}{\tau}\right)$$

4

(1) Green-space cooling intensity (GSCI): representing the modeled cooling magnitude at the equivalent UGS boundary and characterizes the temperature contrast between the UGS boundary and surrounding reference background.

$$\mathrm{GSCI} = \widehat{\mathrm{C}}\Big|_{\rho=\rho_\mathrm{b}} = \mathrm{I}_0 \exp\left(-\frac{1}{2}\rho_\mathrm{b}^2\right)$$

5

(2) Green-space cooling distance (GSCD): representing the modeled radial distance from the equivalent UGS boundary to the cooling-threshold isoline, characterizing the spatial extent of detectable cooling beyond the UGS boundary.

$$\mathrm{GSCD} = \bar{\mathrm{r}}\max\left[\sqrt{\rho_\tau^2} - \sqrt{\rho_\mathrm{b}^2}, 0\right], \bar{\mathrm{r}} = (\mathrm{a}+\mathrm{b})/2$$

6

(3) Green-space cooling efficiency (GSCE): representing the cumulative modeled cooling signal within the effective cooling extent normalized by UGS area, characterizing cooling contribution per unit green-space area. Using the elliptical polar-coordinate area element, GSCE was calculated as:

$$\mathrm{GSCE} = \frac{1}{\mathrm{A}}\int_{\rho_\mathrm{b}}^{\rho_\tau} \widehat{\mathrm{C}}\,\mathrm{hspace}\{0.33\mathrm{em}\}\mathrm{dA} = \frac{2\mathrm{I}_0}{\rho_\mathrm{b}^2}\left[\exp\left(-\frac{1}{2}\rho_\mathrm{b}^2\right) - \exp\left(-\frac{1}{2}\rho_\tau^2\right)\right]$$

7

Note

equations (5)–(7) provide a unified formulation of the three cooling metrics based on the fitted Gaussian surface and the cooling threshold τ.

To evaluate the performance of the anisotropic GSM, representative fitted spatial patterns and fitting accuracy assessments are provided in Supplementary Figs. S2–S3. The goodness of fit was evaluated using the Pearson correlation coefficient (*r*) and root mean square error (RMSE, K), with their distributions summarized across the four ECOSTRESS observations. Most *r* values exceeded 0.7, while RMSE values were concentrated within 1–3 K, indicating generally acceptable agreement between the observed temperature-contrast fields and the fitted GSM surfaces.

3.3 Statistical analysis

To examine associations between explanatory variables and multidimensional UGS cooling, statistical analysis comprised variable screening, RF modeling, and model interpretation. Candidate variables were first examined for completeness and variability, and those with high missing rates or insufficient variance were excluded. Multicollinearity was assessed using variance inflation factors (VIF), with variables exceeding a VIF of 10 excluded [36]. Pearson correlation analysis was then used to identify variables showing significant bivariate associations ($p < 0.05$) with GSCI, GSCD, and GSCE, while physical interpretability was also considered during variable selection. To further reduce predictor redundancy, strongly intercorrelated variables or variables derived from the same source were consolidated, with representative variables retained for subsequent modeling [36].

RF models were fitted separately for each combination of ECOSTRESS observation and cooling metric. This design was adopted because the four observations represented heterogeneous observation windows rather than a continuous temporal sequence, allowing landscape–cooling associations to be compared across both observations and cooling dimensions. Model hyperparameters were optimized using grid search with 10-fold cross-validation. The final models used n_estimators = 500, max_depth = 20, max_features = "sqrt", min_samples_split = 2, and min_samples_leaf = 1, with the random seed fixed at 42 for reproducibility [37]. Model performance was evaluated using the coefficient of determination (R^2), root mean square error (RMSE), and mean absolute error (MAE).

SHAP values were calculated for each fitted RF model to quantify the contribution of explanatory variables to model predictions. Overall feature importance was summarized using mean absolute SHAP values, enabling comparison of variable contributions across observations and cooling dimensions. SHAP beeswarm plots were used to examine the direction and distribution of feature contributions in relation to feature values [38]. For variables with relatively high contributions, partial dependence plots (PDPs) were used to characterize nonlinear marginal responses across their observed ranges [39]. SHAP dependence plots were further used to examine conditional patterns between key variables, with a secondary variable represented by the color gradient to assess how the contribution of the focal variable varied across different structural or contextual conditions [40]. All statistical analyses and machine-learning models were implemented in Python 3.11 using scikit-learn, statsmodels, and SHAP.

4 Results

4.1 Variation in multidimensional UGS cooling and bivariate associations

GSM-derived cooling metrics showed substantial variation in multidimensional UGS cooling across the four ECOSTRESS observations (Fig. 2). The lowest cooling levels were observed at 00:31, with median GSCI, GSCD, and GSCE values of 0.5 K, 130 m, and 1.2 K, respectively; some UGS also exhibited negative GSCI values. Cooling levels were higher at 07:37, with corresponding medians of 1.5 K, 180 m, and 2.2 K. The highest median values occurred at 10:50, reaching 5.5 K for GSCI, 270 m for GSCD, and 6.5 K for GSCE. The distributions at 10:50 were also broader and more right-skewed than those at the other

observations, showing greater heterogeneity among UGS. At 16:37, median GSCI, GSCD, and GSCE values were 3.5 K, 230 m, and approximately 4.0 K, respectively, with narrower distributions than at 10:50. Overall, the three cooling dimensions showed clear differences in both magnitude and distribution across observations.

Pearson correlation analysis showed that the strength, direction, and significance of bivariate associations between explanatory variables and cooling metrics also varied across ECOSTRESS observations (Supplementary Fig. S4). Area_in was significantly and positively correlated with all three cooling metrics across the four observations, representing the most consistently recurring bivariate association. NDVI_in showed stronger correlations at 07:37 and 10:50 and weaker correlations at 00:31 and 16:37. Among internal geometry variables, LSI_in and Cohesion_in showed significant positive correlations with GSCD and GSCE mainly at 07:37 and 10:50. Associations involving morphological variables were more observation-specific: BH_out and FAR_out were significantly negatively correlated with cooling metrics at 07:37, whereas SVF_in and ED_out showed positive correlations. External contextual variables also varied among observations. Albedo_out was negatively correlated with cooling metrics at 10:50 and 16:37 but showed weak positive correlations at 00:31 and 07:37, while NDVI_out was positively correlated with GSCI at 00:31 and showed stronger correlations with GSCD in other observations. Overall, the bivariate results distinguished the recurring positive association of Area_in from the more observation-dependent associations of other internal, morphological, and external contextual variables.

4.2 Consistent and observation-dependent landscape–cooling associations

RF models showed R^2 values above 0.68 across the four ECOSTRESS observations. Mean absolute SHAP values revealed clear differences in the relative contributions of explanatory variables across both cooling dimensions and observations (Fig. 3). Area_in consistently ranked among the most important variables for GSCI, GSCD, and GSCE across all four observations, showing the most recurring contribution among the evaluated variables. NDVI_in also contributed substantially in several models, particularly at 07:37, 10:50, and 16:37 and for GSCE, but its contribution was considerably weaker at 00:31. Among internal geometry variables, Cohesion_in showed relatively high importance at 07:37, whereas the contributions of other geometry-related variables varied across observations and cooling dimensions. Morphological ventilation and external urban-context variables generally showed less recurring importance, with their relative contributions concentrated in particular observations or cooling dimensions. Overall, the SHAP importance patterns distinguished the comparatively recurring contribution of Area_in from the more observation- and dimension-dependent contributions of the remaining explanatory variables.

SHAP value distributions provided additional information on the direction and variability of these contributions (Fig. 4). Area_in was predominantly associated with positive SHAP values across cooling metrics and observations, indicating that its recurring importance was accompanied by a largely

consistent positive contribution to model-predicted cooling. NDVI_in showed stronger positive contributions at 07:37, 10:50, and 16:37, particularly for GSCE at 10:50 and 16:37, while its SHAP values remained closer to zero at 00:31. Cohesion_in was mainly associated with positive contributions at 07:37 and 10:50, whereas PD_in and LSI_in showed more variable or bidirectional contribution patterns in specific observations. Morphological variables also varied in contribution direction across observations; BH_out and FAR_out were predominantly associated with negative SHAP values at 07:37, 10:50, and 16:37, while SVF_in showed a more positive distribution at 00:31. External contextual variables similarly displayed observation-dependent contribution patterns. Together, the SHAP importance and contribution distributions showed that landscape–cooling associations differed in their degree of recurrence across observations and cooling dimensions, with Area_in exhibiting the clearest recurring positive pattern.

4.3 Nonlinear responses and conditional relationships among explanatory variables

PDP analysis revealed widespread nonlinear and observation-dependent marginal responses across cooling dimensions (Fig. 5). Area_in showed a recurring positive association with cooling, but the magnitude of marginal gains generally decreased as green-space area increased. Changes in the marginal response occurred around 20 ha in several models, including GSCI at 10:50 and 16:37, although the subsequent response differed across observations and cooling dimensions. NDVI_in also showed nonlinear responses, with marked changes occurring mainly within the range of approximately 0.4–0.5. At 00:31, its marginal response changed around 0.4, while at 10:50 GSCD increased markedly as NDVI_in rose from approximately 0.4 to 0.5; at 16:37, GSCI and GSCE showed weaker marginal changes above approximately 0.5. Configuration-related variables showed more observation- and metric-specific patterns. LSI_in was positively associated with GSCD under particular observations, Cohesion_in showed a strong positive marginal response for GSCE at 10:50 before leveling off, and PD_in showed negative marginal associations with GSCD and GSCE at 16:37. Overall, nonlinear responses were common, but the location and magnitude of marginal changes varied across variables, cooling dimensions, and observations.

SHAP dependence analysis further showed that the contribution of key landscape attributes varied across combinations of internal structure and surrounding context (Fig. 6). Conditional patterns involving Area_in recurred across several observations, but their magnitude and shape differed with vegetation, spatial configuration, and morphological conditions. At 00:31, Area_in showed stronger positive contributions at larger green-space sizes when combined with higher NDVI_in, while the response gradually leveled off at larger areas. At 07:37, Area_in-related changes in GSCD were concentrated mainly within approximately 20–30 ha, after which marginal changes became smaller. At 10:50, GSCE showed smaller changes when Area_in exceeded approximately 50 ha, whereas at 16:37 the contribution of Area_in to GSCI leveled off beyond approximately 20 ha. Conditional patterns were also evident for vegetation and spatial configuration: higher NDVI_in combined with higher Cohesion_in

was associated with stronger cooling contributions in several models, although the corresponding ranges and magnitudes varied among observations. Associations involving surrounding morphology were less uniform; patterns involving Area_in or NDVI_out varied with SVF_in, and the contribution associated with BH_out differed across levels of SVF_in. Overall, the SHAP dependence patterns showed that landscape–cooling associations were conditional on combinations of explanatory variables rather than being uniformly expressed across their observed ranges.

5 Discussion

5.1 Observation-dependent differences in multidimensional UGS cooling

The four ECOSTRESS observations revealed substantial differences in multidimensional UGS cooling, which should be interpreted as observation-dependent contrasts rather than as a continuous diurnal pattern. Cooling was weakest at 00:31, with some green spaces even exhibiting negative values. Although a single nighttime observation cannot establish a general nocturnal mechanism, the weak cooling at 00:31 is consistent with studies showing that nighttime cooling varies with thermal contrasts between green spaces and surrounding built surfaces and heat release from urban materials [41, 42]. By contrast, stronger daytime cooling is consistent with evidence that radiative forcing, evapotranspiration, and shading enhance surface-temperature contrasts associated with green spaces [43].

Differences among observations also involved the heterogeneity of UGS cooling. The greater spread of all three cooling metrics at 10:50 is consistent with evidence of greater cooling heterogeneity under stronger daytime thermal contrasts [44, 45]. Multi-layered vegetation and favorable ventilation have been associated with longer-distance cooling propagation [22, 46], potentially contributing to the broader GSCD distribution at 10:50; however, these physical processes were not directly examined here. These results indicate that single-window assessments may not fully capture the magnitude or heterogeneity of UGS cooling [47, 48].

5.2 Consistent and observation-dependent landscape associations

The relative contributions of explanatory variables varied across cooling dimensions and ECOSTRESS observations. Blue-green factors and internal geometry generally showed stronger associations with cooling performance, whereas morphological ventilation and external urban context became more relevant under particular dimensions and observations, suggesting more conditional associations [15]. This contrast indicates differing degrees of consistency in landscape–cooling associations: internal landscape attributes were comparatively recurring, whereas morphological and contextual associations were more dependent on observation conditions and cooling dimensions.

At the variable level, key landscape–cooling associations were predominantly nonlinear. Area_in showed diminishing marginal gains with increasing green-space size, consistent with previous evidence of scale dependence in UGS cooling [10, 49]. A change in marginal response around 20 ha recurred in several models, although its magnitude and subsequent response differed across cooling metrics and observations. NDVI_in also showed nonlinear responses, with stronger cooling gains concentrated within intermediate-to-high vegetation ranges, consistent with evidence that vegetation-related cooling may level off at high vegetation levels [50, 51]. Higher Cohesion_in was associated with stronger cooling efficiency and propagation under particular conditions, consistent with evidence that landscape continuity and aggregation can support UGS cooling [12, 52].

SHAP dependence patterns further indicated that landscape–cooling associations varied across combinations of internal structure and surrounding context. In particular, higher NDVI_in combined with higher Cohesion_in was associated with stronger cooling in several models, suggesting that vegetation-related cooling associations may depend partly on spatial continuity [53, 54]. This recurrence supports jointly considering vegetation condition and spatial continuity, while another recurring pattern involved green-space size in combination with surrounding openness and urban context. Associations of Area_in varied with SVF_in and NDVI_out, indicating dependence on the structural and contextual conditions in which green spaces were embedded [15, 55]. These conditional patterns help explain why similar green-space sizes or vegetation conditions may correspond to different cooling outcomes under different structural and contextual settings [56, 57].

5.3 Implications and insights for UGS design

From a planning perspective, landscape attributes showing relatively consistent cooling associations across observations may provide more transferable planning priorities, whereas observation- and context-dependent associations require greater adaptation to local conditions. Green-space size and vegetation condition therefore warrant particular attention. In this study, stronger cooling was generally associated with moderate-to-large green spaces and relatively high vegetation condition within the observed range, consistent with previous evidence on the importance of green-space scale and vegetation characteristics [51, 57]. Maintaining internal spatial continuity may also support cooling, while highly fragmented configurations should be considered cautiously given their potential association with weaker cooling continuity [12]. The repeated nonlinear and conditional patterns further suggest that planning should emphasize coordinated configurations of area, vegetation condition, and spatial cohesion rather than simply maximizing any single attribute.

At a broader spatial scale, the observation-dependent associations of morphological variables indicate that the urban context surrounding UGS should be considered when interpreting cooling propagation. Previous studies suggest that green corridors can support urban heat mitigation through landscape connectivity and cooling propagation [58]. Although this study did not directly simulate airflow, associations involving BH_out, FAR_out, and SVF_in suggest that surrounding urban morphology may condition the expression and spatial extent of UGS cooling [59]. Building height and density around

green-space connections should therefore be considered alongside vegetation continuity and openness rather than translated into a universal configuration.

The interface between UGS and surrounding land uses also warrants attention because adjacent landscape conditions may influence cooling beyond green-space boundaries. Previous research suggests that peripheral vegetation can support cooling continuity and spatial extent [51]. UGS design may therefore benefit from maintaining vegetation continuity between core and peripheral green spaces and limiting extensive impervious surfaces that may interrupt it. Buffer integration should therefore emphasize landscape continuity and reduced abrupt contrasts at the green space–built environment interface rather than a fixed-width prescription. Building form and peripheral green space should be adapted to local morphology and site conditions, with gradual landscape transitions potentially supporting cooling continuity [60].

5.4 Limitations and future prospects

This study provides insights into multidimensional UGS cooling and the consistency and conditionality of its landscape associations across multiple ECOSTRESS observations, but several limitations remain. The study focuses on the BTH urban agglomeration, which is characterized by a warm temperate monsoon climate and relatively concentrated urban patterns and surface properties. The applicability of our conclusions in other climate zones, urban morphologies, and socioeconomic contexts requires further validation. Due to the 70 m spatial resolution and irregular overpass frequency of ECOSTRESS, uncertainties remain in characterizing small-scale UGS and local thermal processes. Moreover, the four ECOSTRESS observations were acquired on different dates and in different years rather than forming a continuous diurnal sequence. Therefore, differences among observations may also reflect variations in background meteorological and surface conditions, and should not be interpreted solely as time-of-day effects. Some explanatory variables still rely on landscape indices or statistical grid data, making it difficult to fully capture fine-scale differences in vegetation structure, micrometeorological disturbances, and energy exchange. Additionally, the interpretation of cooling patterns is primarily based on remote-sensing observations and statistical modeling, which characterize associations and conditional patterns but do not directly resolve process-level energy transfer or microclimatic feedbacks. Future research could test the consistency and transferability of key landscape–cooling relationships and nonlinear response patterns across different climate zones and urban types, improve model accuracy using ground-based or unmanned aerial vehicle thermal infrared observations, and further strengthen understanding of UGS cooling associations through multi-source data fusion.

6 Conclusions

Taking the BTH urban agglomeration as a case study, this study examined how multidimensional UGS cooling performance and its landscape associations varied across multiple ECOSTRESS observations using Gaussian surface modeling and interpretable machine-learning approaches. The results showed that GSCI, GSCD, and GSCE captured complementary dimensions of cooling intensity, extent, and efficiency, with substantial differences in both cooling magnitude and heterogeneity across the four

observations. The lowest cooling values occurred in the 00:31 observation and the highest in the 10:50 observation, while the distributions of the three metrics also differed across observations. These findings indicate that UGS cooling performance should not be treated as a fixed property captured by a single observation window.

Landscape–cooling associations differed in their degree of consistency across ECOSTRESS observations and cooling dimensions. Area_in exhibited the most recurring SHAP importance across the three cooling metrics and four observations, while the contributions of NDVI_in and Cohesion_in varied more across cooling dimensions and observations. Morphological and external contextual factors showed greater observation dependence. This distinction suggests that landscape attributes identified as important under individual observations should not automatically be assumed to provide equally consistent cooling-related evidence across different observational settings.

The relationships between key landscape attributes and UGS cooling were predominantly nonlinear and conditional. Area_in repeatedly showed diminishing marginal gains, with changes in marginal response occurring around 20 ha in several models, while NDVI_in showed marked response changes mainly around 0.4–0.5 rather than a uniform increase across its full range. SHAP dependence patterns further showed that associations involving vegetation condition, spatial cohesion, green-space size, and surrounding morphology varied across structural and contextual combinations. These findings support a differentiated planning approach: comparatively recurring associations, particularly those involving green-space scale, may inform broader planning priorities, while vegetation condition, spatial continuity, and surrounding morphology should be considered in coordinated and context-sensitive configurations rather than translated into uniform design prescriptions.

Declaration of generative AI and AI-assisted technologies in the manuscript preparation process

During the preparation of this work, the authors used ChatGPT (OpenAI) to assist with language polishing and readability. After using this tool, the authors reviewed and edited the content as needed and take full responsibility for the content of the published article.

Abbreviations

UGS
Urban green spaces
LST
Land surface temperature
ECOSTRESS
NASA ECOSTRESS mission
GSCI
Green-space cooling intensity
GSCD
Green-space cooling distance

GSCE
Green-space cooling efficiency
BTH
Beijing–Tianjin–Hebei
GSM
Gaussian surface model
RF
Random forest
SHAP
Shapley additive explanations
PDP
Partial dependence plot

Declarations

Competing Interests

The authors declare that they have no known competing financial interests or personal relationships that could have appeared to influence the work reported in this paper.

Author Contribution

X.J. conceived the study, developed the methodology, conducted data analysis, performed visualization, and wrote the original draft. J.P. contributed to research supervision, project administration, funding acquisition, and manuscript revision. H.W. contributed to research supervision, funding acquisition, and manuscript revision. J.L. contributed to data processing, analysis, and manuscript revision. W.Z. contributed to data interpretation and manuscript revision. Y.Y. contributed to data processing and manuscript revision. All authors reviewed and approved the final manuscript.

Data Availability

The datasets used in this study include publicly available remote sensing and geospatial datasets, which can be accessed from their respective data providers as described in the manuscript. The derived datasets supporting the findings of this study are available from the corresponding author upon reasonable request, subject to applicable third-party data access restrictions.

References

1. Mentaschi, L. et al. Global long-term mapping of surface temperature shows intensified intra-city urban heat island extremes. *Glob Environ. Change*. **72**, 102441 (2022).
2. Huang, Y. et al. Association between urban heat islands and heat-related mortality in 70 pairs of adjacent urban-rural counties among 8 topographic regions in China. *Sustain. Cities Soc.* **121**, 106182 (2025).
3. Vanos, J. et al. A physiological approach for assessing human survivability and liveability to heat in a changing climate. *Nat. Commun.* **14**, 7653 (2023).
4. Wu, Z., Shi, Y., Ren, L. & Hang, J. Scaled outdoor experiments to assess impacts of tree evapotranspiration and shading on microclimates and energy fluxes in 2D street canyons. *Sustain. Cities Soc.* **108**, 105486 (2024).
5. Balany, F., Ng, A. W. M., Muttil, N., Muthukumaran, S. & Wong, M. S. Green infrastructure as an urban heat island mitigation strategy—a review. *Water* **12**, 3577 (2020).
6. Li, Z., Wang, Z., Wen, D. & Wu, L. How urban parks and their surrounding buildings affect seasonal land surface temperature: a case study in Beijing, China. *Urban Urban Green.* **87**, 128047 (2023).
7. Yan, M., Chen, L., Leng, S. & Sun, R. Effects of local background climate on urban vegetation cooling and humidification: variations and thresholds. *Urban Urban Green.* **80**, 127840 (2023).
8. Lin, Z. et al. Day and night: impact of 2D/3D urban features on land surface temperature and their spatiotemporal non-stationary relationships in urban building spaces. *Sustain. Cities Soc.* **108**, 105507 (2024).
9. Wei, Z. et al. Diurnal variations in cooling effects of urban parks based on ECOSTRESS data: a case study of Beijing. *Urban Clim.* **58**, 102229 (2024).
10. Xu, Z. & Zhao, S. Scale dependence of urban green space cooling efficiency: a case study in Beijing metropolitan area. *Sci. Total Environ.* **898**, 165563 (2023).
11. Zhang, J., Zhang, H. & Qi, R. A study of size threshold for cooling effect in urban parks and their cooling accessibility and equity. *Sci. Rep.* **14**, 16176 (2024).
12. Li, Y., Ren, C., Ho, J. Y. & Shi, Y. Landscape metrics in assessing how the configuration of urban green spaces affects their cooling effect: a systematic review of empirical studies. *Landsc. Urban Plan.* **239**, 104842 (2023).
13. Xiong, Y., Xie, X. & Yang, Y. Evaluation and optimization of park cooling benefits based on cumulative impact and landscape pattern. *Sci. Rep.* **14**, 25092 (2024).
14. Zhang, Y., Wang, Y., Ding, N. & Yang, X. Spatial pattern impact of impervious surface density on urban heat island effect: a case study in Xuzhou, China. *Land* **11**, 2135 (2022).
15. Chen, Z., Ye, J., Liu, Y., Hu, T. & Dong, J. Global assessment in the effect of urban built-up environment on cooling efficiency of green spaces. *Commun. Earth Environ.* **6**, 968 (2025).
16. Liu, Z. et al. Nonlinear cooling effect of street green space morphology: evidence from a gradient boosting decision tree and explainable machine learning approach. *Land* **11**, 2220 (2022).

17. Shen, Y. et al. Stereoscopic urban morphology metrics enhance the nonlinear scale heterogeneity modeling of UHI with explainable AI. *Urban Clim.* **56**, 102006 (2024).
18. Hong, T., Yim, S. H. L. & Heo, Y. Interpreting complex relationships between urban and meteorological factors and street-level urban heat islands: application of random forest and SHAP method. *Sustain. Cities Soc.* **126**, 106353 (2025).
19. Wu, X., Wang, L., Yao, R., Luo, M. & Li, X. Identifying the dominant driving factors of heat waves in the north China plain. *Atmos. Res.* **252**, 105458 (2021).
20. Zeng, L., Yang, L., Su, L., Hu, H. & Feng, C. The impact of policies on land use and land cover changes in the Beijing–Tianjin–Hebei region in China. *Environ. Impact Assess. Rev.* **110**, 107676 (2025).
21. Zhang, X. et al. GLC_FCS10: a global 10 m land-cover dataset with a fine classification system from Sentinel-1 and Sentinel-2 time-series data in Google Earth Engine. *Earth Syst. Sci. Data*. **17**, 4039–4062 (2025).
22. Gallay, I., Olah, B., Murtinová, V. & Gallayová, Z. Quantification of the cooling effect and cooling distance of urban green spaces based on their vegetation structure and size as a basis for management tools for mitigating urban climate. *Sustainability* **15**, 3705 (2023).
23. Qiu, X. et al. Cooling effect of urban blue and green spaces: a case study of Changsha, China. *Int. J. Environ. Res. Public. Health*. **20**, 2613 (2023).
24. Wang, M., Song, H., Zhu, W. & Wang, Y. The cooling effects of landscape configurations of green–blue spaces in urban waterfront community. *Atmosphere* **14**, 833 (2023).
25. Wang, L., Wang, G., Chen, T. & Liu, J. The regulating effect of urban large planar water bodies on residential heat islands: a case study of Meijiang Lake in Tianjin. *Land* **12**, 2126 (2023).
26. Mushore, T. D., Mutanga, O. & Odindi, J. Determining the influence of long term urban growth on surface urban heat islands using local climate zones and intensity analysis techniques. *Remote Sens.* **14**, 2060 (2022).
27. Hulley, G. & Freepartner, R. *ECOSTRESS Mission Level 2 Product User Guide V002 (JPL D-103137)*. (2024).
28. Chang, Y. et al. Exploring diurnal thermal variations in urban local climate zones with ECOSTRESS land surface temperature data. *Remote Sens. Environ.* **263**, 112544 (2021).
29. Hu, T. et al. Continental-scale evaluation of three ECOSTRESS land surface temperature products over Europe and Africa: temperature-based validation and cross-satellite comparison. *Remote Sens. Environ.* **282**, 113296 (2022).
30. Cai, X., Yang, J., Zhang, Y., Xiao, X. & Xia, J. Cooling island effect in urban parks from the perspective of internal park landscape. *Humanit. Soc. Sci. Commun.* **10**, 674 (2023).
31. Zhu, W. et al. How to measure the urban park cooling island? A perspective of absolute and relative indicators using remote sensing and buffer analysis. *Remote Sens.* **13**, 3154 (2021).
32. Streutker, D. R. A remote sensing study of the urban heat island of Houston, Texas. *Int. J. Remote Sens.* **23**, 2595–2608 (2002).

33. Anniballe, R., Bonafoni, S. & Pichierri, M. Spatial and temporal trends of the surface and air heat island over Milan using MODIS data. *Remote Sens. Environ.* **150**, 163–171 (2014).
34. Keeratikasikorn, C. & Bonafoni, S. Satellite images and gaussian parameterization for an extensive analysis of urban heat islands in Thailand. *Remote Sens.* **10**, 665 (2018).
35. Gao, Z., Zaitchik, B. F., Hou, Y. & Chen, W. Toward park design optimization to mitigate the urban heat island: assessment of the cooling effect in five U.S. cities. *Sustain. Cities Soc.* **81**, 103870 (2022).
36. Dormann, C. F. et al. Collinearity: a review of methods to deal with it and a simulation study evaluating their performance. *Ecography* **36**, 27–46 (2013).
37. Probst, P., Wright, M. N. & Boulesteix, A. L. Hyperparameters and tuning strategies for random forest. *WIREs Data Min. Knowl. Discov*. **9**, e1301 (2019).
38. Lundberg, S. M. & Lee, S. I. A Unified Approach to Interpreting Model Predictions. in *Advances in Neural Information Processing Systems 30* 1–10Curran Associates, Inc., Long Beach, CA, USA, (2017).
39. Friedman, J. H. Greedy function approximation: a gradient boosting machine. *Ann. Stat.* **29**, 1189–1232 (2001).
40. Lundberg, S. M., Erion, G. G. & Lee, S. I. Consistent Individualized Feature Attribution for Tree Ensembles (arXiv:1802.03888). Preprint at (2019). https://doi.org/10.48550/arXiv.1802.03888
41. Shu, M., Lu, Y., Chen, R., Chen, K. & Lin, X. Study on the diurnal difference of the impact mechanism of urban green space on surface temperature and sustainable planning strategies. *Sustainability* **17**, 10193 (2025).
42. Martin, M., Ramani, V. & Miller, C. InfraRed investigation in Singapore (IRIS) observatory: urban heat island contributors and mitigators analysis using neighborhood-scale thermal imaging. *Energy Build.* **307**, 113973 (2024).
43. Li, H. et al. Cooling efficacy of trees across cities is determined by background climate, urban morphology, and tree trait. *Commun. Earth Environ.* **5**, 754 (2024).
44. Sun, F. et al. Study on Microclimate and Thermal Comfort in Small Urban Green Spaces in Tokyo, Japan—A Case Study of Chuo Ward. *Sustainability* **15**, 16555 (2023).
45. Vo, T. T. & Hu, L. Diurnal evolution of urban tree temperature at a city scale. *Sci. Rep.* **11**, 10491 (2021).
46. Zhang, Y. & Dai, M. Analysis of the cooling and humidification effect of multi-layered vegetation communities in urban parks and its impact. *Atmosphere* **13**, 2045 (2022).
47. Peng, J. et al. Response of urban green space cooling effect to urbanization in the three ring road area of Changsha City. *Sustain. Cities Soc.* **109**, 105534 (2024).
48. Stumpe, B., Stuhrmann, N. & Marschner, B. Variability of cooling distances and intensities of urban green spaces over six hot summer days affects their relevance for UHI mitigation in Berlin, Germany. *Sustain. Cities Soc.* **137**, 107139 (2026).

49. Yan, Z. et al. The scale-dependent differences in cooling efficiency of UGS in different functional areas: a case study of Xi'an, China. *Forests* **15**, 1946 (2024).
50. Simović, I., Radulović, M., Dunjić, J., Savić, S. & Šećerov, I. Influence of urban greenery on microclimate across temporal and spatial scales. *Forests* **16**, 1729 (2025).
51. Soltanifard, H. & Amani-Beni, M. The cooling effect of urban green spaces as nature-based solutions for mitigating urban heat: insights from a decade-long systematic review. *Clim. Risk Manag*. **49**, 100731 (2025).
52. Zhang, K. et al. Discover the desirable landscape structure of urban parks for mitigating urban heat: a high spatial resolution study using a forest city, Luoyang, China as a lens. *Int. J. Environ. Res. Public. Health*. **20**, 3155 (2023).
53. Zhang, Y., Wang, Y., Ding, N. & Yang, X. Assessing the contributions of urban green space indices and spatial structure in mitigating urban thermal environment. *Remote Sens.* **15**, 2414 (2023).
54. Kumar, M., Bhadwal, S. & Sahu, N. Role of urban green space structure and configuration in regulating land surface temperature in NCT Delhi using explainable artificial intelligence. *Urban Clim.* **65**, 102736 (2026).
55. Yan, L., Jia, W. & Zhao, S. The cooling effect of urban green spaces in metacities: a case study of Beijing, China's Capital. *Remote Sens.* **13**, 4601 (2021).
56. Bai, D., Miao, C., Xi, Y., Liu, H. & He, C. The impact of 2D/3D building morphology and green spaces on urban heat environments: relative contributions, interaction and marginal effects. *Ecol. Indic.* **180**, 114296 (2025).
57. Zhang, J., Wang, P. & Jin, A. Multidimensional characteristics of urban green space and its impact in mitigating urban heat island effects: a case study of Guangzhou. *Sci. Rep.* **15**, 39959 (2025).
58. Molina-Barrenechea, I., Véliz-Rojas, M. F. & Ibáñez-Blancas, A. N. & la Torre-Cuadros, M. de los Á. Effect of green corridors on the mitigation of the urban heat island (UHI) in the district of Lince, Lima, Peru. *Atmósfera* 39, 383–399 (2025).
59. Fang, Y. & Gu, K. Review of urban ventilation corridor research: characteristics and progress. *Acta Ecol. Sin*. **44**, 5444–5458 (2024).
60. Zhang, L., Bagan, H., Chen, C. & Yoshida, T. Exploring the impact of urban morphology on river cooling effects: A case study of the Arakawa river in Tokyo. *Ecol. Indic.* **172**, 113288 (2025).

Figures

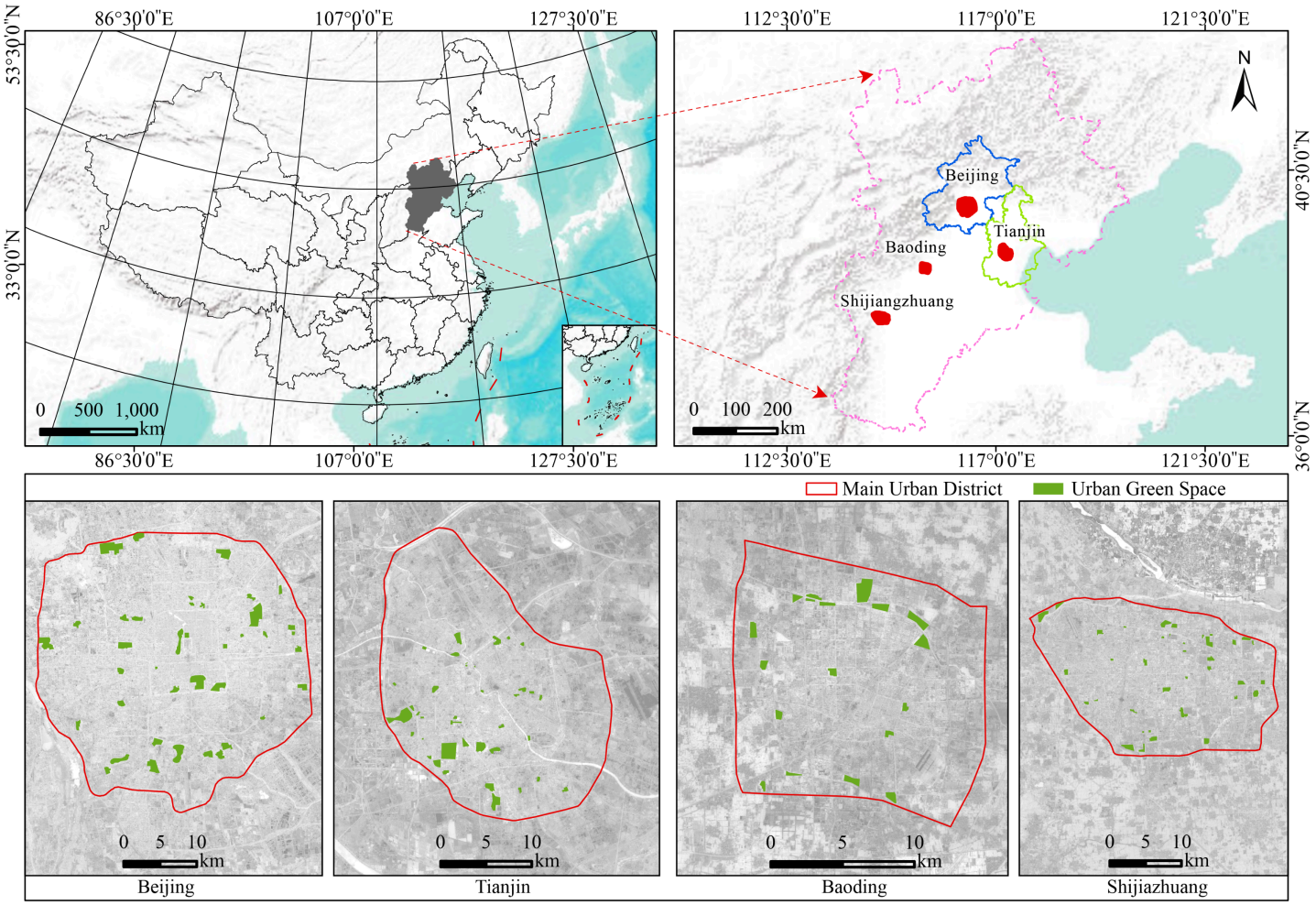


Figure 1

Location of the study area and distribution of UGS samples.

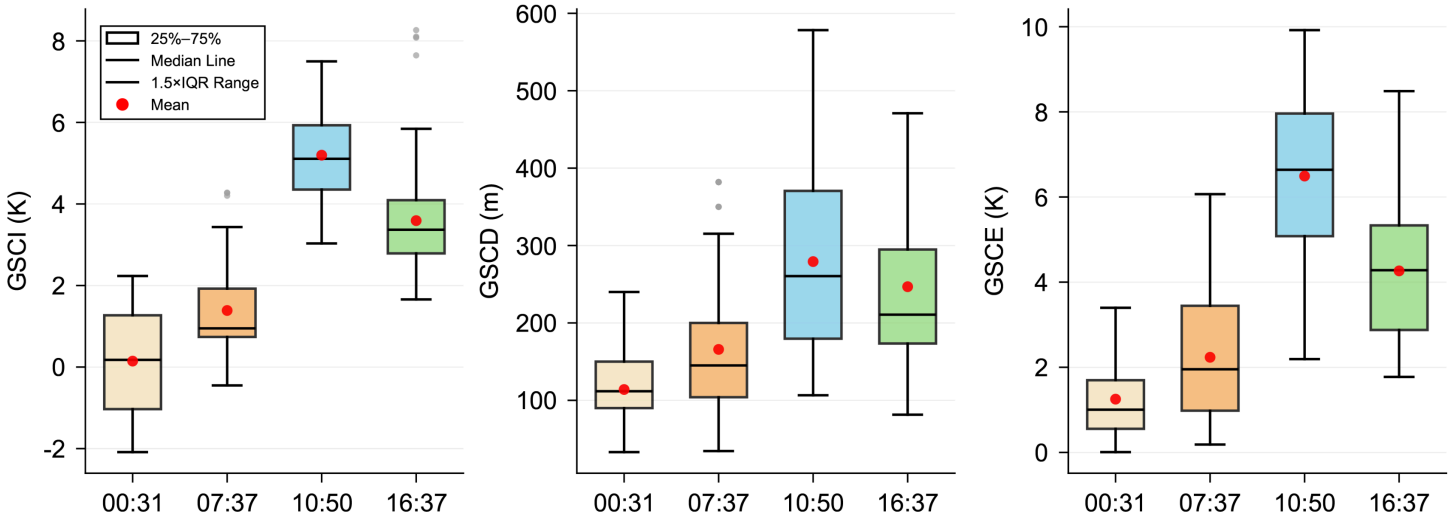


Figure 2

GSCI, GSCD, and GSCE across the four ECOSTRESS observations.

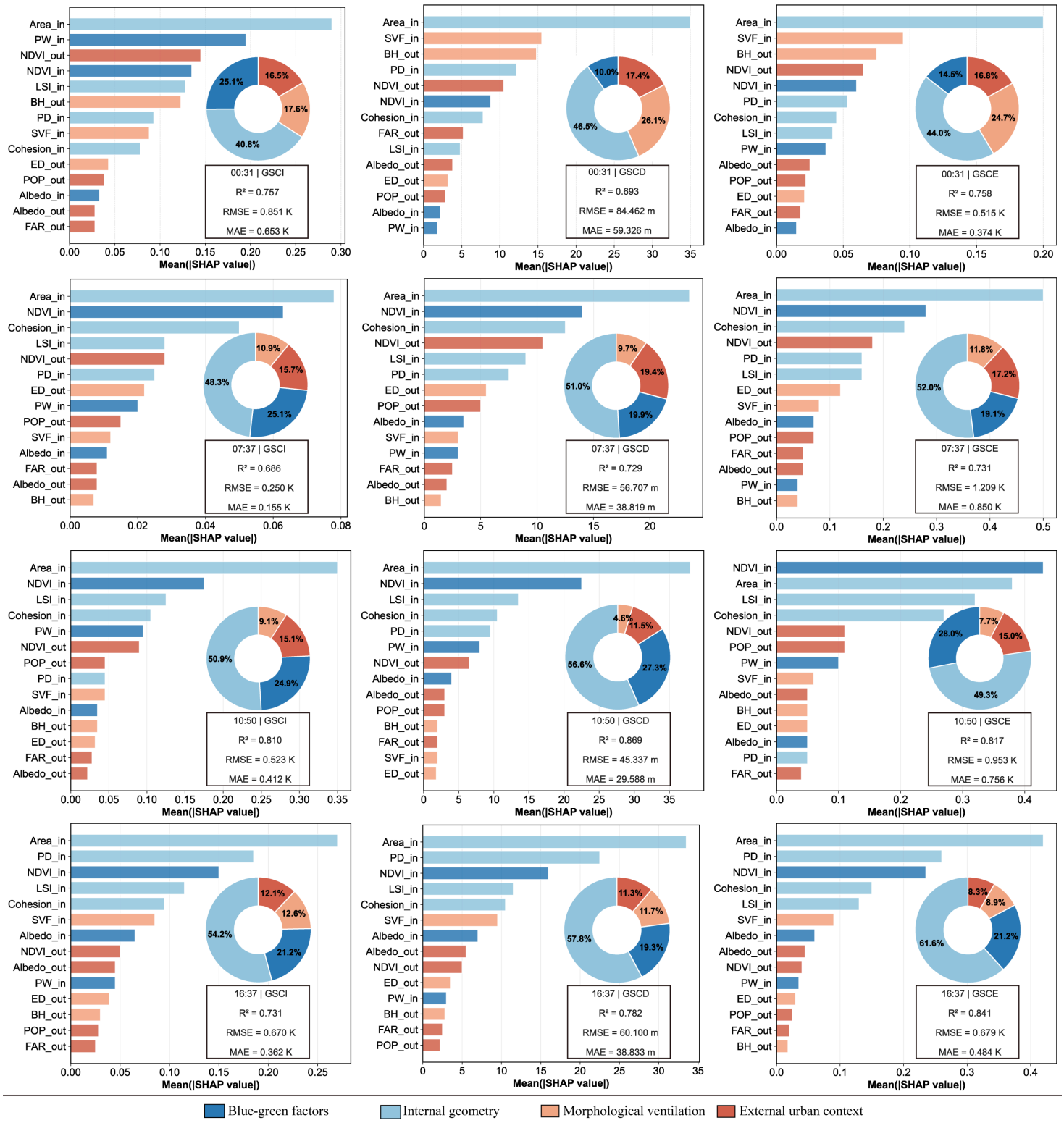


Figure 3

SHAP-based feature importance across three cooling metrics and four ECOSTRESS observations.

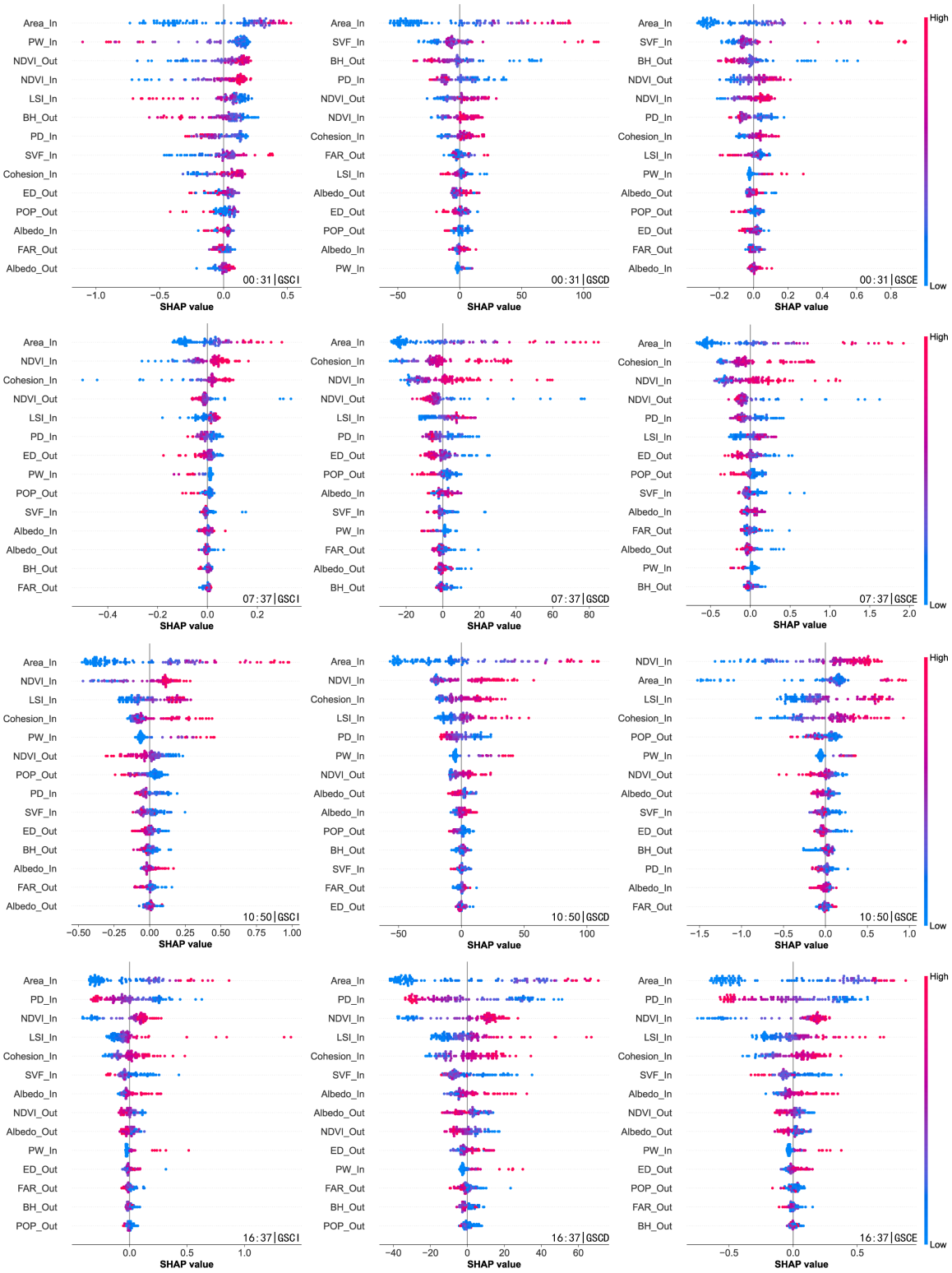


Figure 4

SHAP beeswarm plots showing feature contribution distributions across three cooling metrics and four ECOSTRESS observations. Each point represents a UGS sample, with color indicating the feature value (blue: low, red: high) and horizontal position indicating its SHAP contribution to the model output.

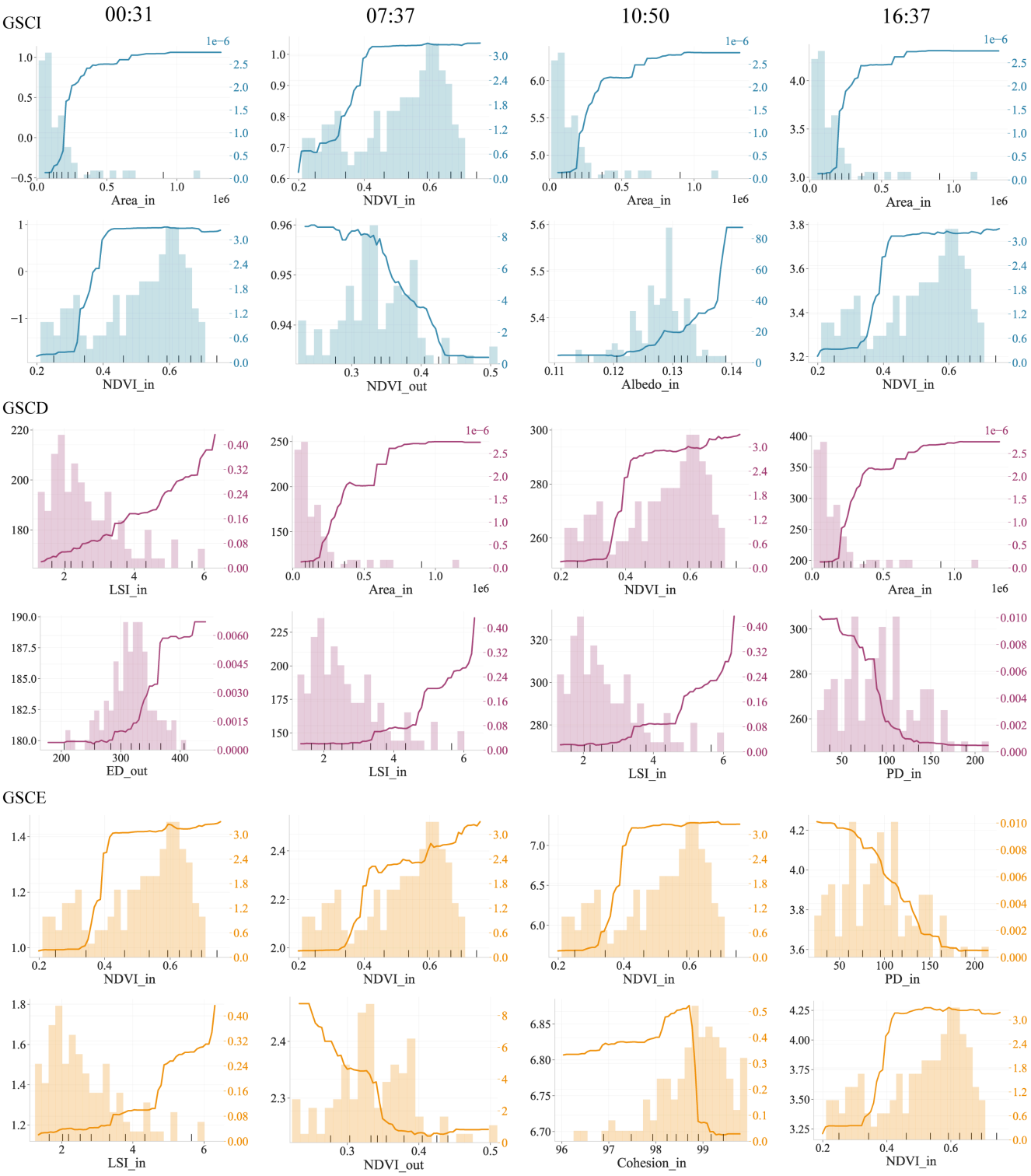


Figure 5

Partial dependence plots showing nonlinear marginal responses of key variables across three cooling metrics and four ECOSTRESS observations. Lines indicate averaged marginal responses, and histograms show the distributions of the corresponding variables.

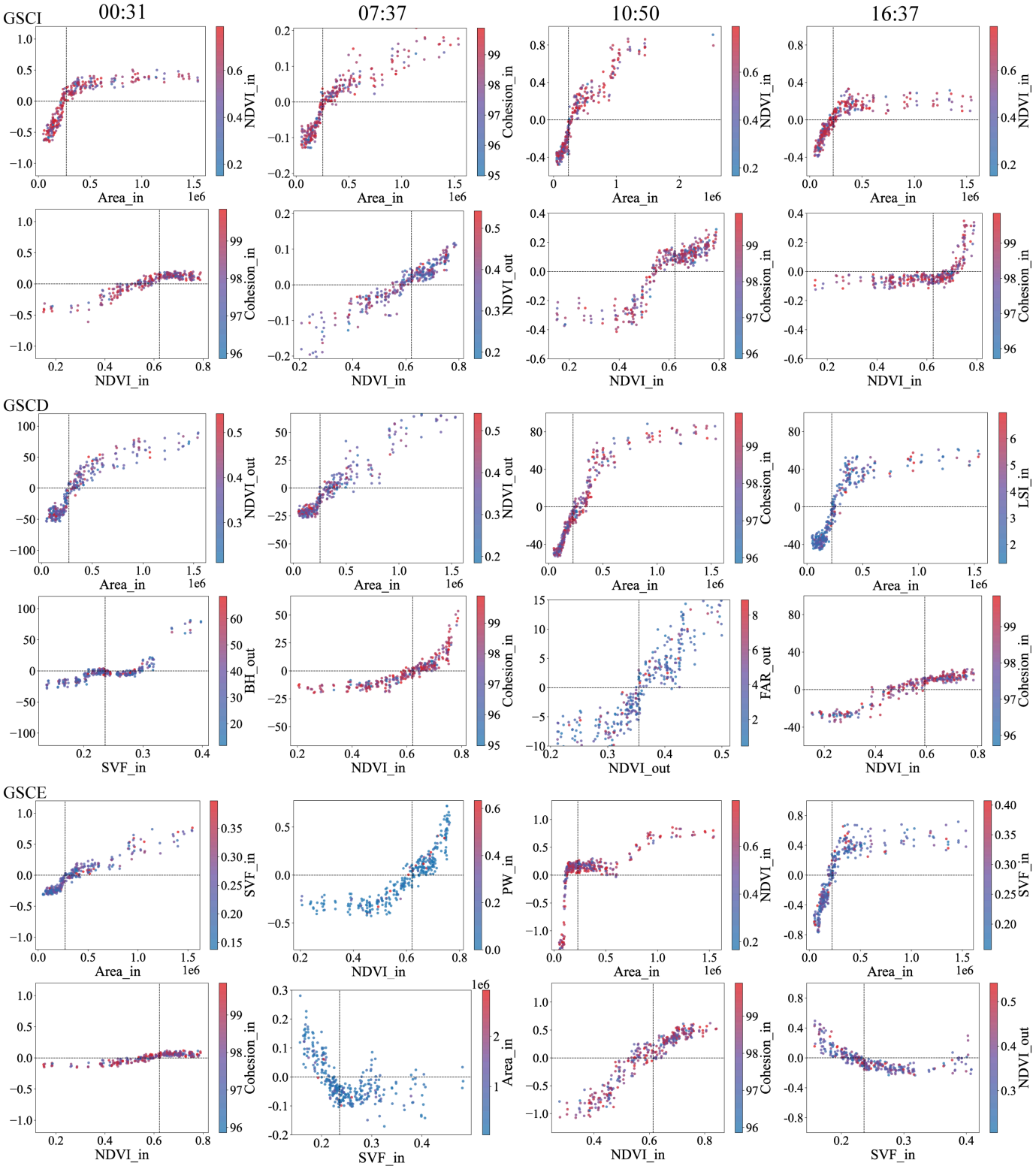


Figure 6

SHAP dependence plots illustrating conditional relationships among key variables across four ECOSTRESS observations. Each panel shows how the SHAP contribution of a focal variable varies across its observed values, with color representing a secondary variable. Nonlinear and joint patterns illustrate how landscape–cooling associations vary under different structural and contextual conditions.

Supplementary Files

This is a list of supplementary files associated with this preprint. Click to download.

- SupplementaryInformation.pdf